Desalination and Water Treatment
www.deswater.com

doi: 10.5004/dwt.2021.26515

209 (2021) 170–181
January

Adsorptive behavior of biochar and zinc chloride activated hydrochar prepared from *Acacia leucophloea* wood sawdust: kinetic equilibrium and thermodynamic studies

Samiyappan Nirmaladevi*, Pachagoundanpalayam Nachimuthu Palanisamy

Centre for Environmental Research, Department of Chemistry, Kongu Engineering College, Perundurai, Erode-638 060, Tamil Nadu, India, Tel. +91 9486636176; email: devinks86@gmail.com (S. Nirmaladevi), Tel. +91 9750264390; email: asppavithran@gmail.com (P.N. Palanisamy)

Received 29 December 2019; Accepted 29 August 2020

ABSTRACT

In the present study, two adsorbents, namely biochar (BC) and $ZnCl_2$ activated hydrochar (ZAHC) are prepared from *Acacia leucophloea* wood sawdust. BC is prepared by direct pyrolysis of the sawdust at 700°C while ZAHC is prepared by two-stage process, which includes hydrothermal carbonization to produce hydrochar followed by chemical activation with $ZnCl_2$. The structural properties of the adsorbents prepared are characterized by Fourier-transform infrared spectroscopy, Brunauer–Emmett–Teller surface area and point zero charge. The adsorption performance of the prepared BC and ZAHC toward anionic dye, acid blue 15 is evaluated by batch mode studies. The study shows that the isotherm data are found to fit with Langmuir and fairly with Freundlich and Temkin isotherms. Likewise, kinetics data are found to fit with the pseudo-second-order kinetic model. The adsorbents exhibit favorable surface area of 1,380 and 550 m^2g^{-1} for ZAHC and BC respectively. Therefore they can be used as adsorbents for the removal of dyes from aqueous solutions.

Keywords: Activated carbon; Adsorption; Wood sawdust; Hydrochar; High surface area; Biochar

1. Introduction

Nowadays, synthetic dyes are used widely in many fields. However, their discharge into water gives undesirable color to the water body which would reduce sunlight penetration and affect aquatic life. Various methods such as adsorption, coagulation, advanced oxidation and membrane separation are used in the treatment of dyes containing wastewater [1]. Among these, adsorption is one of the most effective techniques to remove the color from wastewater [2]. Commercial activated carbons are utilized by textile industries for the treatment of dye wastes. However, there is a great interest to search for effective and low-cost alternatives to the existing commercial activated carbon. Recently, agricultural biomass has attracted much attention owing to its wide availability. Therefore, low-cost adsorbent, if developed from agricultural biomass, can be used to treat the pollution of water by textile industries at a reasonable cost. In this regard, dry pyrolysis and wet pyrolysis are promising approaches for the preparation of char material from biomasses [3].

In dry pyrolysis, the raw material is heated at high temperatures (400°C–1,200°C) in an inert atmosphere or in a non-circulated air atmosphere to produce biochar. In contrast, in wet pyrolysis, also known as hydrothermal carbonization, the raw materials are taken in an autoclave containing a given solution at 150°C–350°C for 2–24 h to produce hydrochar [4,5]. Similar to activated carbon, biochar may act

* Corresponding author.

1944-3994/1944-3986 © 2021 Desalination Publications. All rights reserved.

as an effective adsorbent for pollutant removal due to its high degree of porosity and large surface area. However, its adsorption efficiency depends on the raw material and pyrolysis conditions [6]. Further, the application of hydrochars for environmental protection is limited due to their low porosity, poor surface area and low adsorption ability [7]. Therefore chemical modification of hydrochar would enhance its capacity to remove pollutants. The higher adsorption capacity of chemically modified hydrochar is reported in the literature [8–11].

Acacia leucophloea (commonly known as white-bark acacia) is abundantly available in arid regions of India. It is used for indoor construction, flooring and although a little hard to work, for furniture. It is also used as firewood (*source*: www.worldagroforestry.org). Hence the sawdust produced from this wood in large quantities is disposed of as waste. In recent years, the sawdust from different species of wood such as rubber wood, eucalyptus, cedar wood and teak has been considered as the feedstock for the preparation of activated carbon [12]. To the best of knowledge, no studies are available in the literature regarding the preparation of biochar (BC) and activated hydrochar (ZAHC) from *Acacia leucophloea* wood sawdust (ALWSD) for the removal of dyes from aqueous solutions. Hence, in the present study, this material is chosen as a lignocellulosic precursor due to its huge availability in nature, renewable and thus low-cost biomass. Therefore the present study aims to prepare ALWSD based adsorbents by dry and wet pyrolysis to produce biochar and hydrochar respectively and chemical activation of hydrochar by $ZnCl_2$. The characteristics of BC and ZAHC and their adsorption performance towards acid blue 15 (AB15) in terms of kinetics, isotherms and thermodynamics are presented.

2. Materials and methods

2.1. Materials

Acid blue 15 (molecular formula = $C_{42}H_{46}N_3NaO_6S_2$, molecular weight = 775.96; purity = 95% absorbance maximum (λ_{max}): 560 nm) is purchased from local dye suppliers. The stock solutions (1,000 mg L^{-1}) of AB15 are prepared by dissolving accurately the weighed amount of the dye in distilled water. All the working AB15 dye solutions are prepared by diluting the stock solution with distilled water. All the chemicals used in this study are of analytical-grade and used without purification.

2.2. Preparation of BC

ALWSD is collected from local sawmills and used as a precursor. The wood sawdust is washed with water to remove adhering impurities. Then it is dried in an oven at 100°C for 24 h, ground and sieved to obtain a particle size of the range of 150 μ. BC is prepared from ALWSD via direct pyrolysis. The pyrolysis process is executed in a muffle furnace (Sigma-High temperature furnace, Chennai) under oxygen-limited conditions. Approximately, 20 g of ALWSD is taken in a silica crucible covered with a lid and heated in a muffle furnace at a rate of 10°C/min until 700°C, held at this temperature for 2 h and allowed to cool at room temperature. The biochar produced is treated with dil.HCl to remove ash and inorganic salts, then washed in distilled water and dried at 100°C. Later, it is ground with mortar and pestle, labeled as BC. Further, it is used for characterization and adsorption studies.

2.3. Preparation of ZAHC

The preparation of ZAHC from ALWSD is published in our recent publication [13]. In a typical experiment, approximately, 15 g of the ALWSD is mixed with 50mL of distilled water in a 100 mL Teflon-lined autoclave. Then the autoclave is placed in a muffle furnace and heated at a rate of 10°C/min until 210°C, held at this temperature for 6 h under self-generated pressure and then allowed to cool to room temperature. The hydrochar obtained is washed with distilled water and then placed in an oven at 105°C for drying. The activated carbon is synthesized from the chemical activation of hydrochar with $ZnCl_2$. In this study, the impregnation ratio is calculated as the ratio of the weight of $ZnCl_2$ in solution to the weight of the hydrochar prepared. $ZnCl_2$/hydrochar impregnation ratio is varied between 1:1 and 8:1. Ten to eighty grams of $ZnCl_2$ have been dissolved in 150 mL of dissolved water and then 10 g of hydrochar is mixed with the solution. The mixture has been left for 6 h at room temperature. Then the liquid portion is filtered and the remaining solids have been subjected to dryness at 110°C in a hot oven for about 24 h. Approximately 10 g of impregnated hydrochar is taken in a silica crucible covered with a lid and carbonized under an oxygen-limited environment. The operating conditions for the activated carbon preparation from hydrochar have been determined by studying the effect of impregnation ratio (1:1, 2:1, 4:1, 6:1, 8:1 $ZnCl_2$/hydrochar, W/W), carbonization temperature (500°C, 600°C, 700°C and 800°C) and carbonization time (0.5, 1.0 and 2 h). The activated carbon produced at better operating condition is referred to as ZAHC. Finally, ZAHC is washed with dil.HCl until the pH of the filtrates reaches a constant value and then in distilled water. The sample is then dried and kept in a tightly-closed container for dye treatment.

2.4. Material characterization

Information about the functional groups present in ZAHC and BC is obtained by Fourier-transform infrared spectroscopy (FTIR, Perkin Elmer, USA) and the textural property is measured by N_2 adsorption–desorption isotherms at 77K (Autosorb-1, Quantachrome). The point zero charge (pH_{PZC}) values of the adsorbents are determined by using the drift method reported in the literature [5].

2.5. Adsorption performance of AB15

The adsorptive performance of BC and ZAHC towards AB15 is evaluated by batch mode adsorption studies. Experiments are conducted in a series of 250 mL Erlenmeyer flasks containing 50 mL of AB15 solution. The flasks are agitated in an orbital shaker (REMI, RIS-24BL) with a fixed shaking speed of 170 rpm. The effect of adsorbent dose and pH (2–9) on the adsorption process is studied to determine the optimum conditions for the removal of AB15 by ZAHC

and BC. The pH of the AB15 solution is adjusted by adding 0.1 M HCl or 0.1 M NaOH. The final concentration of the AB15 solution is measured by a UV-visible spectrophotometer (Elico DR3900, Hyderabad) at a wavelength of λ_{max} = 560 nm.

The quantity of the dye adsorbed q_e (mg g^{-1}) and removal (%) is determined as follows.

$$q_e = \frac{(C_0 - C_e)V}{m} \quad (1)$$

where V is the solution volume (L), m is the mass of adsorbent (g) and C_0 and C_e are the initial and the equilibrium concentrations of AB15 (mg L^{-1}) respectively.

$$\%\ \text{of dye removal} = \left(\frac{C_0 - C_e}{C_0}\right) \times 100 \quad (2)$$

2.6. Adsorption kinetics

The adsorption dynamics are analyzed to identify the required equilibration time [14] and to study the adsorption process, whether the process is chemical or physical adsorption [15]. In the current study, four kinetic models such as pseudo-first-order (PFO), pseudo-second-order (PSO), Elovich equation and intraparticle diffusion model are selected to describe the adsorption kinetics.

The PFO equation [16] is expressed as:

$$\text{Log}\left(q_e - q_t\right) = -\frac{K_1}{2.303}t + \log\left(q_e\right) \quad (3)$$

where q_e (mg g^{-1}) and q_t (mg g^{-1}) are the adsorption amounts of AB15 for ZAHC and BC at equilibrium and at time t(min) respectively while K_1 (min^{-1}) is the PFO equation rate constant. The value of q_e and (K_1) is calculated from the intercept and the slope of the linear plot of log ($q_e - q_t$) vs. t.

The PSO equation [16] is as follows.

$$\frac{t}{q_t} = \left(\frac{1}{q_t}\right)t + \frac{1}{q_e^2 K_2} \quad (4)$$

where K_2 (g mg^{-1} min^{-1}) is the pseudo-second-order rate constant. Linear plot of t/q_t vs. t would give the value of (K_2) and q_e.

Elovich kinetic model [15] is represented by the following equation.

$$q_t = \frac{1}{\beta}\ln(t) + \frac{1}{\beta}\ln(\alpha\beta) \quad (5)$$

where α (mg g^{-1} min^{-1}) is the initial adsorption rate constant and β (mg g^{-1}) is the desorption constant. The values of α and β are calculated from the slope and the intercept of the linear plot of q_t vs. ln(t).

Intraparticle diffusion [16] is expressed as follows.

$$q_t = K_p\sqrt{t} + C \quad (6)$$

where K_p (mg g^{-1} min$^{-1/2}$) is the intraparticle diffusion model rate constant and C (mg g^{-1}) is a constant associated with the thickness of the boundary layer. Further, the value of K_p and C is calculated directly from the slope and the intercept of the linear plot of q_t vs. $t^{1/2}$.

The activation energy E_a (kJ mol^{-1}) of the adsorption process can be used to predict whether the adsorption is physical or chemical and it is calculated using the Arrhenius equation. The following equation describes the activation energy calculated based on kinetic studies conducted at two temperatures.

Arrhenius equation:

$$K = Ae^{-Ea/RT} \quad (7)$$

$$\ln\frac{K_{2(323K)}}{K_{2(303K)}} = \frac{E_a}{R}\left(\frac{1}{T_1} - \frac{1}{T_2}\right) \quad (8)$$

where $K_{2(323K)}$ and $K_{2(303K)}$ are the rate constants of the pseudo-second-order model at 323 and 303 K respectively, A is the pre-exponential factor, R is the universal gas constant (8.314 J mol^{-1} K^{-1}) and T is the absolute temperature in Kelvin.

2.7. Adsorption isotherm

Adsorption isotherms are helpful to elucidate the adsorption mechanisms. In the current study, three isotherm models including Langmuir, Freundlich and Temkin models are selected to study the adsorption behavior. The linearized form of the Langmuir model [17] is shown in the equation.

$$\frac{C_e}{q_e} = \left(\frac{1}{Q^0_{max}}\right)C_e + \frac{1}{Q^0_{max}K_L} \quad (9)$$

where Q^0_{max} (mg g^{-1}) is the maximum saturated monolayer adsorption capacity of an adsorbent, C_e (mg L^{-1}) is the adsorbate concentration at equilibrium, q_e (mg g^{-1}) is the amount of adsorbate adsorbed at equilibrium and K_L (L mg^{-1}) is the Langmuir constant.

Freundlich's model [18] is represented by the following equation.

$$\log q_e = n\log C_e + \log K_F \quad (10)$$

where K_F (mg g^{-1}) is the Freundlich's constant and n is the measure of the effectiveness of the adsorption process.

The Temkin equation [19] is represented as follows.

$$q_e = B\ln A + B\ln C_e \quad (11)$$

where $B = RT/b$, R is the universal gas constant (8.314 J mol^{-1} K^{-1}) and T is the absolute temperature in K, B is related to the heat of adsorption and A is the equilibrium binding constant (L mg^{-1}).

2.8. Adsorption thermodynamics

Adsorption thermodynamic studies are conducted to understand the feasibility and nature of the adsorption

process. Thermodynamic parameters such as $\Delta G°$, $\Delta S°$ and $\Delta H°$ can be calculated according to the law of thermodynamics as follows.

$$\Delta G° = -RT \ln K \quad (12)$$

$$\Delta G° = \Delta H° - T\Delta S° \quad (13)$$

The van't Hoff equation is given as follows.

$$\ln K = \frac{-\Delta H°}{R} \times \frac{1}{T} + \frac{\Delta S°}{R} \quad (14)$$

where R is the gas constant, K is the equilibrium constant calculated from the isotherm model that provides the best fit [20] and T is the temperature (K). The value of $\Delta G°$ can be calculated directly from Eq. (14) while $\Delta H°$ and $\Delta S°$ are determined from the slope and the intercept of a plot ln$K$ against 1/T.

3. Results and discussion

3.1. Characterization

3.1.1. Fourier-transform infrared spectroscopy

To determine the surface functional groups on ZAHC and BC, the samples are subjected to FTIR analysis. The FTIR spectra of ZAHC and BC before and after adsorption are shown in Fig. 1. BC and ZAHC display characteristics bands at the wavelength around 3,450 cm^{-1} which may be ascribed to O–H bonds in alcohol, phenol and absorbed water molecules. In addition, both BC and ZAHC show a very weak band in the region around 2,880 cm^{-1} which is attributed to the aliphatic C–H stretching vibration. The band at around 1,630 cm^{-1} in BC and ZAHC may be due to the C=O group. The region around 1,200–1,400 cm^{-1} may be due to C=O and C–H bonds, which can belong to alcohol, ester and aromatic groups. Thus, the existence of potential binding sites in BC and ZAHC of different nature is confirmed by FTIR spectra. The FTIR spectra of AB15-bounded ZAHC reveals significant variations in their peak wavelength, for instance, the broadband at 3,504; 3,472 and 3,400 cm^{-1} may be due to bonded O–H group. The peak at 2,880 cm^{-1} in ZAHC disappears after the adsorption of AB15 and a new peak is observed at 1,119 cm^{-1}. The peaks at 1,631 and 1,266 cm^{-1} shifted to 1,627 and 1,384 cm^{-1}, respectively. Similarly, AB15 bonded BC exhibits broad bands at 3,511 and 3,330 cm^{-1} corresponding to bonded –OH group. The peaks at 2,917 cm^{-1} in BC shifted to 2,910 cm^{-1} and the peak at 1,627 cm^{-1} shifted to 1,574 cm^{-1}. Therefore the change in FTIR spectra of BC and ZAHC after the adsorption of AB15 is owing to the possible involvement of several functional groups during adsorption.

3.1.2. Characterization of pore structure

Figs. 2a–c show N_2 adsorption–desorption isotherms (77 K) and the pore characteristic (inset graph) of ALWSD, BC and ZAHC. The pore volume and pore diameter of ALWSD are not presented because the experimental error involved in their determination is substantial due to

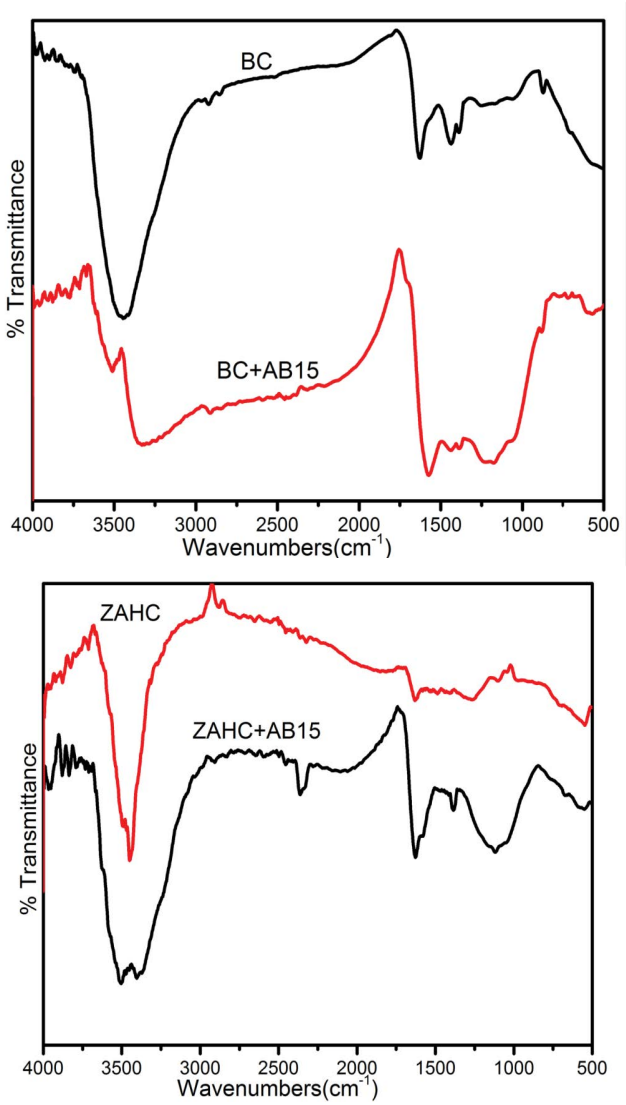

Fig. 1. Fourier-transform infrared spectroscopy of (a) BC and (b) ZAHC before and after AB15 adsorption.

the very small surface area [21]. It can be seen that a low amount of N_2 adsorbed by ALWSD shows isotherm characteristics for low porosity material while ZAHC and BC show an isotherm type I of the International Union of Pure and Applied Chemistry (IUPAC) classification. The type I isotherm is a typical characteristic of microporous materials with a small external surface area [14]. In addition, BC shows a hysteresis loop (wide knee) in its adsorption–desorption isotherm at a relative pressure above 0.3, which is associated with mesoporous structure [14]. The pore characteristics of ALWSD, ZAHC and BC are shown in Table 1. The average pore diameter of the activated carbons prepared confirms the mesoporous structure according to the IUPAC classification. The Brunauer–Emmett–Teller (BET) surface area values of ZAHC and BC obtained in this study have been compared with the other biomass-derived adsorbents reported in the literature and the results are summarized in Table 2.

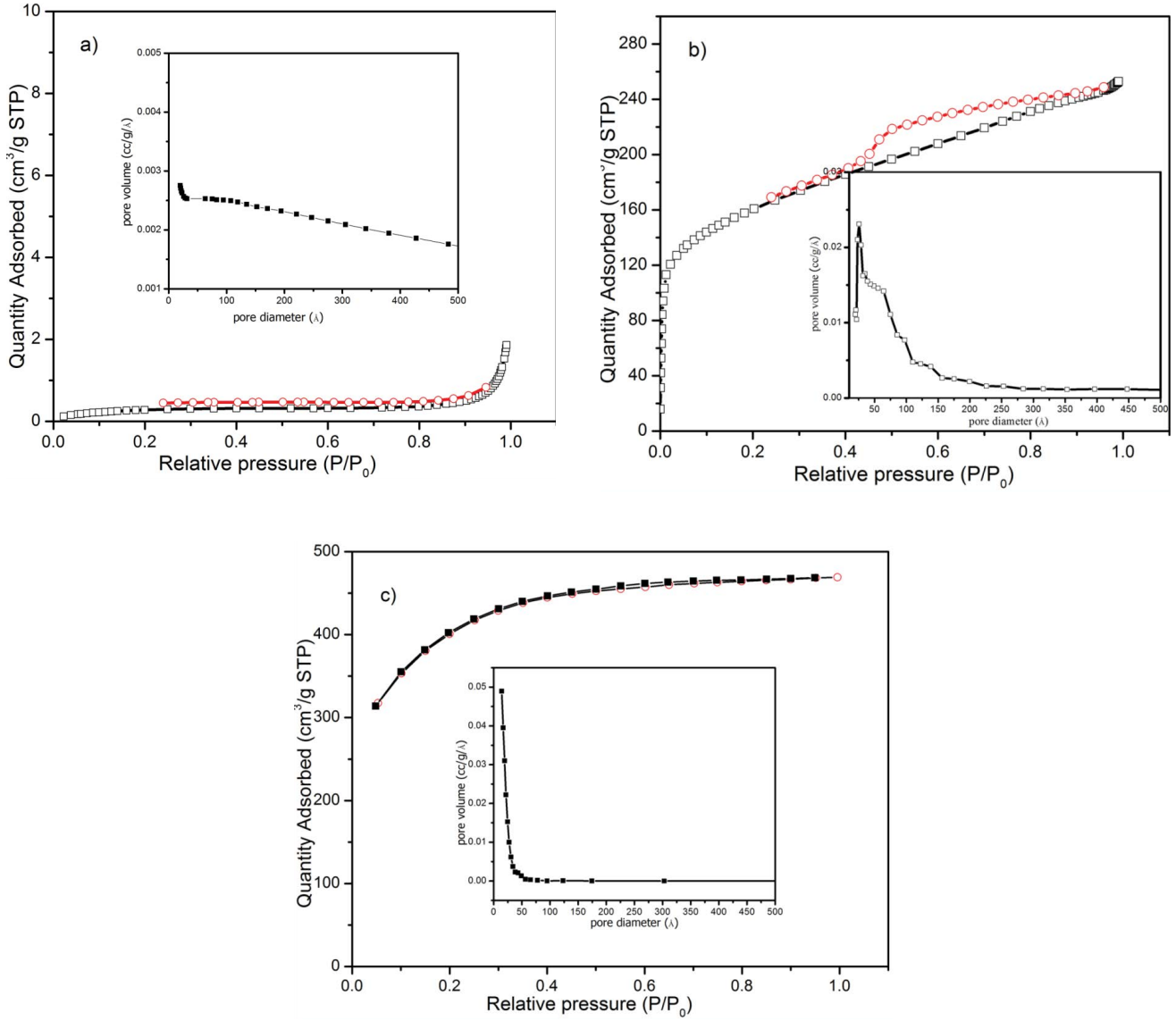

Fig. 2. N_2 adsorption–desorption isotherm and pore size distribution (inset graph) curve of (a) ALWSD, (b) BC and (c) ZAHC.

Table 1
BET characterization results of ALWSD, ZAHC and BC

Materials	S_{BET} ($m^2\ g^{-1}$)	$V\mu$ ($cm^3\ g^{-1}$)	V_M ($cm^3\ g^{-1}$)	Pore diameter (Å)
ALWSD	1.0	–	–	–
ZAHC	1,380	0.589	0.138	21.09
BC	550	0.091	0.299	40.78

S_{BET} – BET specific surface area; $V\mu$ – micropore volume; V_M – mesopore volume.

3.1.3. Effect of adsorbent dosage

The effect of adsorbent doses on the AB15 adsorption and removal efficiency is analyzed by varying the dosage of ZAHC and BC from 25 to 200 mg and the results obtained are shown in Fig. 3. It can be observed that the percentage of dye removal increases with the increase in ZAHC and BC dosages from 25 to 50 mg, but remains almost constant thereafter. This is mainly due to the increase in the number of adsorption sites available for adsorption with the increasing adsorbent dosage. However, the adsorption capacity q_e is decreased from 67 to 11 mg g^{-1} and from 83 to 12 mg g^{-1} for ZAHC and BC respectively when the adsorbent dose is

Table 2
Comparison of BET surface area of the prepared ZAHC and BC with the other adsorbents

Adsorbent	S_{BET} (m^2 g^{-1})	References
Biochar		
Coconut shell	536	[12]
Orange peel	565	[12]
Acacia leucophloea wood sawdust (ALWSD)	550	This study
Activated carbon		
Orange peel	1,025	[12]
Waste potato residue	1,357	[22]
Coffee husks	965	[23]
Rice straw	1,154	[24]
Sunflower oil cake	240	[25]
Waste tea	854	[26]
Tomato waste	1,093	[27]
Rattan sawdust	1,083	[28]
Rattan furniture wastes	1,135	[11]
Cotton stalk	765	[29]
Banana peel	1,188	[30]
Acacia leucophloea wood sawdust (ALWSD)	1,380	This study

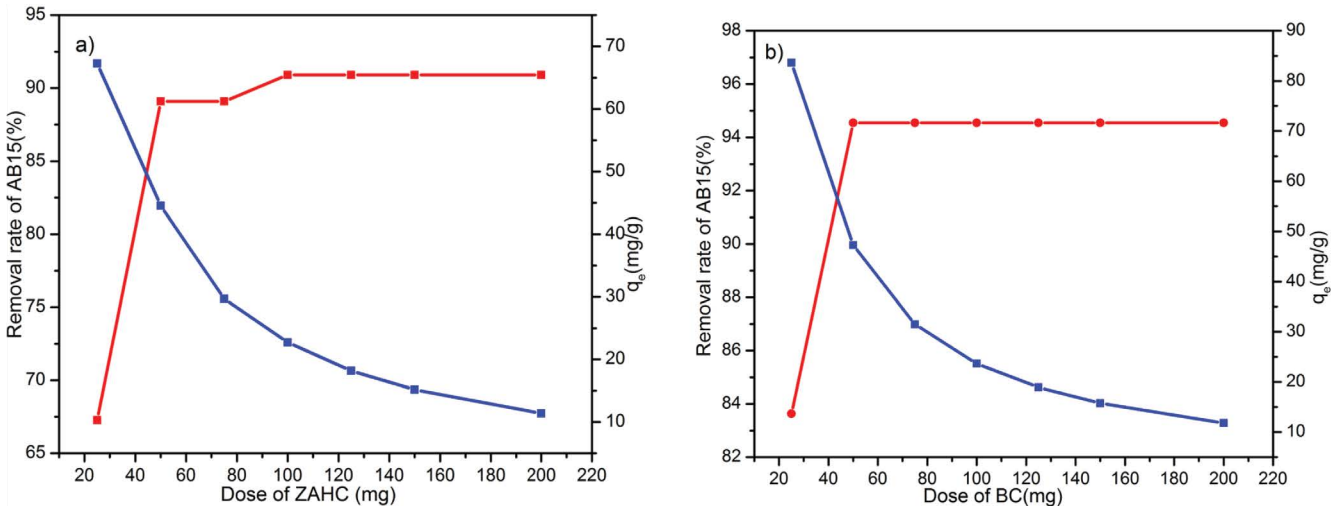

Fig. 3. Effect of adsorbent dosages on the adsorption of AB15 (a) dose of ZAHC and (b) dose of BC (C_0 = 50 mg L^{-1}; V = 50 mL).

increased from 25 to 200 mg. This decrease in adsorption capacity is due to the split in the concentration gradient between solute concentration in the solution and on the surface of the adsorbent [31]. Thus, with the increasing adsorbent dose, the quantity of dye adsorbed onto the unit mass of adsorbent is decreased and hence it leads to a decrease in the adsorption capacity.

3.1.4. Effect of pH

The UV-Vis spectra for different pH of AB15 solutions are measured as shown in Fig. 4a. From the spectra, it is clear that the absorbance of AB15 maximizes at pH (2–9), but minimizes when the solution pH is 10 and above. This decrease in absorbance indicates that the structural change in AB15 occurs at higher pH (pH > 10) which reduces the dye intensity. Similar findings are reported for the adsorption of brilliant green (BG) by peat [32]. Therefore, pH > 10 is not included in this study. pH_{PZC} is the pH where the adsorbent net surface charge corresponds to zero, and it helps to explain the electrostatic forces of attraction between the adsorbent and the adsorbate [11]. Fig. 4b indicates the pH_{PZC} of BC (8.6) and ZAHC (7.6). Based on the pH_{PZC} values, ZAHC and BC can be classified into the H-carbons (pH_{PZC} > 7.0) [5]. Fig. 4c describes the effect of pH (2–9) vs. the percentage of AB15 removal

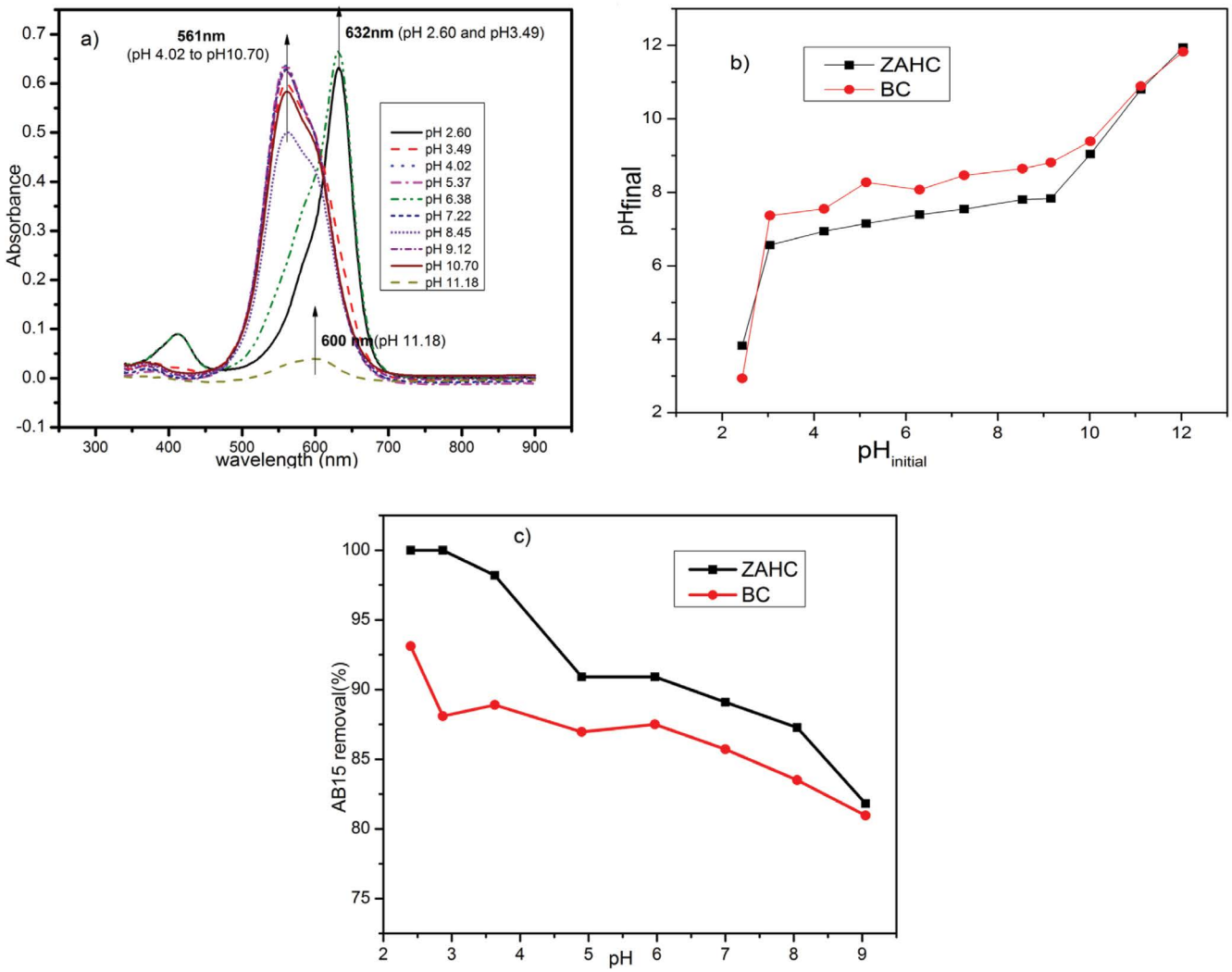

Fig. 4. (a–c) Effect of pH of the AB15 solution on λ_{max} values, zero point charge of ZAHC and BC and pH vs. percentage of AB15 removal of ZAHC and BC (C_0 = 50 mg L^{-1}; dose = 0.5 g).

using ZAHC and BC. It can be seen that when the pH is increased, the adsorption performance decreases from 100% to 80% and from 93% to 80% for ZAHC and BC respectively. It can be explained that at lower pH, the pH_{PZC} of adsorbents becomes positively charged (pH at 7.6, 8.6 and below) so they tend to attract the negatively charged dye species. With the increase in pH, the decrease in AB15 removal is observed as electrostatic repulsion prevails at higher pH.

3.2. Adsorption kinetics

The kinetic curves and parameters calculated for AB15 adsorption onto ZAHC and BC for the three initial concentrations (60, 80 and 100 mg L^{-1}) are shown in Fig. 5 and Table 3. On the basis of high R^2 value (R^2 = 0.999), the pseudo-second-order model is found to be the best one to describe the kinetics of AB15 adsorbed onto ZAHC and BC. Moreover, the calculated q_e values ($q_{e,cal.}$) for the pseudo-second-order model are closer to the experimental q_e ($q_{e,exp.}$) values for all the initial dye concentrations studied. Hence it could be concluded that the pseudo-second-order model is more suitable to explain the adsorption kinetics. In addition, the low E_a values 0.98 kJ mol^{-1} for BC and 17.35 kJ mol^{-1} for ZAHC confirm that the actual adsorption may involve physical adsorption. The low E_a values also indicate that equilibrium can be attained rapidly [14] and the positive E_a values confirm that the adsorption process is endothermic in nature.

3.3. Isotherm study

To evaluate the maximum adsorption capacity of the adsorbents prepared, isotherm experiments are carried out at 300, 310 and 320 K. In the present study, the three adsorption isotherm models like Langmuir, Freundlich and Temkin are utilized to correlate isotherm data and the parameters calculated are presented in Table 4. The Langmuir and Freundlich adsorption isotherms are shown in Fig. 6. The values of regression coefficients are used as the fitting criteria to find the applicability of the three models

Table 3
Kinetic parameters of AB15 adsorption onto ZAHC and BC

Kinetic models	AB15 (mg L^{-1})	Parameters	ZAHC	BC
Pseudo-first-order model	60	$q_{e,cal.}$ (mg g^{-1})	29.34	4.91
		K_1 (min^{-1})	0.0459	0.0557
		R^2	0.9844	0.6523
	80	$q_{e,cal.}$ (mg g^{-1})	23.90	11.91
		K_1 (min^{-1})	0.0635	0.0469
		R^2	0.9861	0.9458
	100	$q_{e,cal.}$ (mg g^{-1})	14.88	30.45
		K_1 (min^{-1})	0.0444	0.1026
		R^2	0.9123	0.9786
Pseudo-second-order model	60	$q_{e,cal.}$ (mg g^{-1})	57.47	54.98
		$q_{e,exp.}$ (mg g^{-1})	52.73	54.55
		K_2 (g mg^{-1} min^{-1})	0.0025	0.0415
		R^2	0.9981	0.999
	80	$q_{e,cal.}$ (mg g^{-1})	64.31	75.59
		$q_{e,exp.}$ (mg g^{-1})	61.82	74.55
		K_2 (g mg^{-1} min^{-1})	0.0053	0.0143
		R^2	0.9996	0.999
	100	$q_{e,cal.}$ (mg g^{-1})	69.74	94.25
		$q_{e,exp.}$ (mg g^{-1})	68.18	91.82
		K_2 (g mg^{-1} min^{-1})	0.0069	0.008
		R^2	0.9998	0.999
Intraparticle diffusion model	60	K_p (mg g^{-1} $min^{-1/2}$)	3.6277	0.8442
		C (mg g^{-1})	23.4414	48.9201
		R^2	0.9338	0.8037
	80	K_p (mg g^{-1} $min^{-1/2}$)	2.4382	1.8114
		C (mg g^{-1})	42.5746	61.7663
		R^2	0.8999	0.9664
	100	K_p (mg g^{-1} $min^{-1/2}$)	2.0503	3.8329
		C (mg g^{-1})	51.7210	66.4486
		R^2	0.8134	0.8858
Elovich kinetic model	60	α (mg g min^{-1})	38.37	4.0738×10^{14}
		β (mg g^{-1})	0.1070	0.6810
		R^2	0.989	0.9223
	80	α (mg g min^{-1})	1,698	27,164
		β (mg g^{-1})	0.1576	0.2656
		R^2	0.977	0.9614
	100	α (mg g min^{-1})	21,727	13,393.68
		β (mg g^{-1})	0.1829	0.1215
		R^2	0.933	0.9446

in explaining the adsorption process. It is found that for ZAHC (R^2 = 0.9352–0.9793), the Langmuir model fits better than the other two models, indicating that the adsorption of AB15 onto ZAHC may be monolayer and the distribution of active sites on the adsorbent is homogeneous [3]. Based on the R^2 value (R^2 = 0.8069–0.8163) Freundlich model fits for BC for the whole range of concentrations (10–100 mg L^{-1}) than the other two models indicating the multilayer adsorption of AB15 onto BC. Moreover, the heterogeneity factor $n < 1$ (ranges from 0.78 to 0.81) indicates that the adsorption process is favorable [14]. The maximum adsorption capacity of AB15 onto ZAHC (40 mg g^{-1}) and BC (84 mg g^{-1}) obtained by Langmuir isotherm at 27°C is compared with the other adsorbents reported in the literature as shown in Table 5.

3.4. Adsorption thermodynamics

The thermodynamic parameters calculated are presented in Table 6. The negative value of ΔG° for all the studied temperatures indicates that the adsorption is favorable and spontaneous. This observation is in good agreement with the calculated R_L value for ZAHC and Freundlich exponent

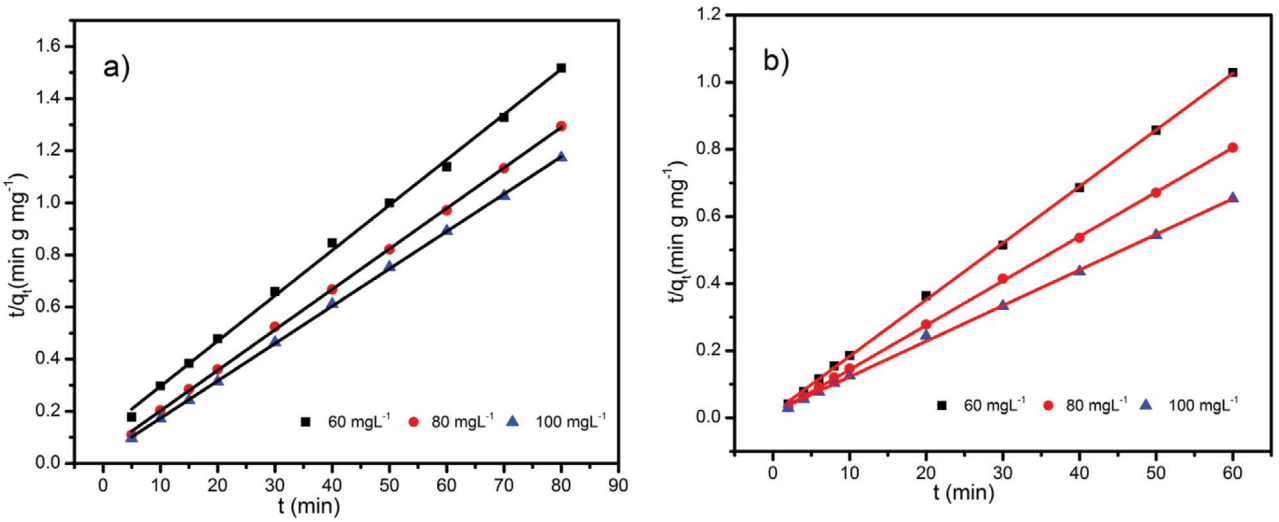

Fig. 5. Pseudo-second-order kinetic model for AB15 adsorption onto (a) ZAHC and (b) BC.

Table 4
Isotherm parameters of AB15 adsorption onto ZAHC and BC

Isotherms models	Parameters	Values at 300 K		Values at 310 K		Values at 320 K	
		ZAHC	BC	ZAHC	BC	ZAHC	BC
Langmuir	Q^0_{max} (mg g^{-1})	40.88	84.43	49.00	83.09	47.48	84.21
	K_L (L mg^{-1})	0.3624	0.3625	0.4109	0.3597	2.6309	0.3405
	R^2	0.9352	0.3368	0.9724	0.3393	0.9793	0.3403
Freundlich	K_F (mg g^{-1}) (mg L^{-1})$^{-1/n}$	0.0813	0.0437	–0.5935	0.0433	0.1324	0.0440
	n	0.2546	0.8147	1.2883	0.7981	0.2826	0.7871
	R^2	0.2895	0.8163	0.4183	0.8073	0.3790	0.8069
Temkin	A (mg g^{-1})	1,434	1.85	1,434	1.90	1,674	1.93
	B	5.93	29.14	7.00	28.33	2.51	28.0
	R^2	0.3397	0.6673	0.5449	0.6499	0.3876	0.6571

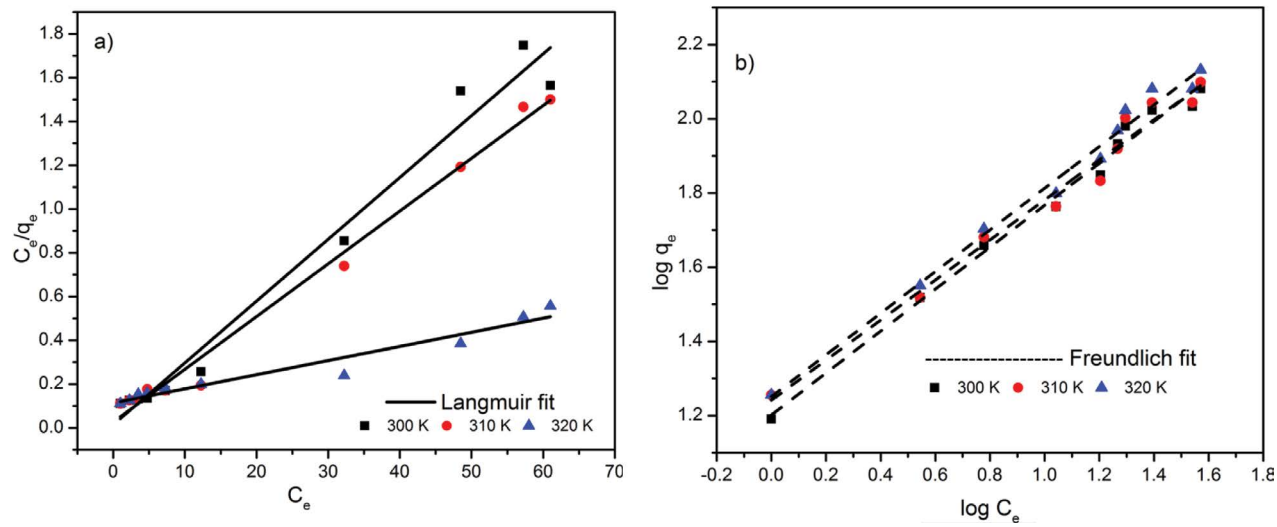

Fig. 6. Adsorption isotherm of AB15 adsorption onto (a) ZAHC and (b) BC.

Table 5
Comparison of the adsorption capacity q_m (mg g^{-1}) of various adsorbents for different acid blue dyes under various conditions

Adsorbent	Dyes	Maximum adsorption capacity q_m (mg g^{-1})	References
$ZnCl_2$ activated hydrochar prepared ALWSD	Acid blue 15	40.88	This study
Biochar prepared ALWSD (BC)	Acid blue 15	84.43	This study
Peat	Acid blue 25	14.4	[33]
Hazelnut shell	Acid blue	60.2	[34]
K_2CO_3-activated olive pomace boiler ash	Acid blue 29	38.48	[35]
Parthenium leaves ash	Acid blue 193	11.75	[36]
Cow dung ash	Acid blue 193	3.85	[36]
Mango stone ash	Acid blue 193	7.59	[36]
Base-treated *Shorea dasyphylla* sawdust	Acid blue 25	24.4	[37]
Azolla pinnata	Acid blue 25	50.5	[38]
Soyabean waste	Acid blue 25	38.3	[38]

Table 6
Thermodynamic parameters for the adsorption of AB15 by ZAHC and BC

Adsorbent	T (K)	$\Delta G°$ (kJ mol^{-1})	$\Delta H°$ (kJ mol^{-1})	$\Delta S°$ (J mol^{-1} K^{-1})
ZAHC	300	–129.23	51.35	180.58
	310	–161.72	63.14	224.87
	320	–131.12	48.52	179.64
BC	300	–158.97	69.24	228.21
	310	–160.06	69.72	229.78
	320	–158.97	69.24	228.22

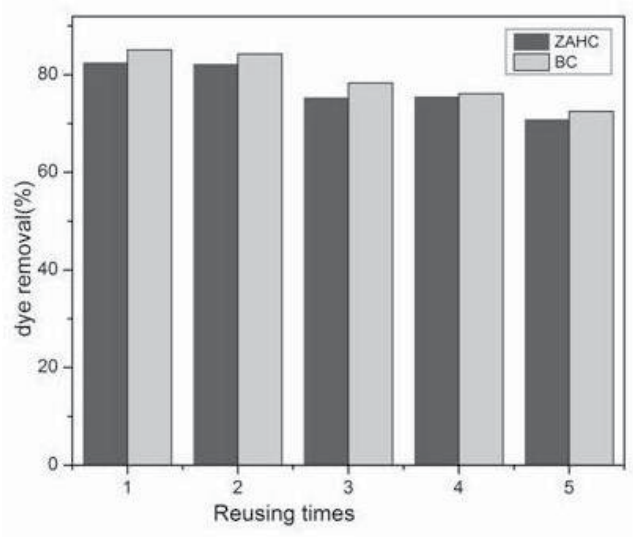

Fig. 7. Desorption studies using ZAHC and BC for the removal of AB15.

n for BC. The positive $\Delta H°$ values indicate the endothermic nature of the process and the values are within the range of (1–93 kJ mol^{-1}) confirming the physisorption [39]. From these results, it is clear that the adsorption of AB15 onto ZAHC and BC may involve physisorption. In addition, positive $\Delta S°$ confirms more randomness at the solid-solution interface.

3.5. Proposed adsorption mechanism

The adsorption mechanism of AB15 can be explained by taking the electrostatic attraction between the adsorbate and the adsorbents. This can be explained by the pH dependence of the adsorption of AB15 onto the adsorbents prepared. Under acid condition when the pH decreases (pH 2 or 3), the adsorbents are positively charged. In contrast, the anionic dye AB15 has a negative sign due to the presence of several sulfonated groups. Therefore the negatively charged dye molecules are attracted by the positively charged adsorbent surfaces, thereby increasing the percentage of dye removal. The same trend is reported in the literature [40,41] for anionic dyes. At higher pH, the adsorbent surface becomes negatively charged and the repulsion between the adsorbent surface and the dye molecule results in a decreased percentage of dye removal. Hence it is clear that most of the AB15 dye uptake processes involve electrostatic force of attraction.

3.6. Reusability studies

Desorption studies also are performed to check the possibility of regeneration of the adsorbents used. Desorption of AB15 is done by using the solvent washing method

in which ZAHC and BC are washed with acidic ethanol. The data for adsorption-desorption experiments are presented in Fig. 7. ZAHC and BC show favorable results up to four cycles and after the fourth cycle, they result in 70% efficiency in dye removal. Hence the results of the adsorption–desorption cycle confirm the reusability of adsorbents for the removal of AB15.

4. Conclusion

In the current study, ALWSD is used successfully to produce activated carbon and biochar. The adsorption efficiency of the adsorbents prepared is tested towards the aqueous solution of AB15. The adsorption process is dependent on the solution pH (2–9). The kinetic studies reveal that the pseudo-second-order model fits well for both the adsorbents and the adsorption requires only low activation energies (0.98–17.35 kJmol^{-1}). The calculated thermodynamic parameters show that AB15 adsorption onto ZAHC and BC occurs spontaneously is endothermic and the positive $\Delta S°$ shows increased randomness. The study shows that ALWSD can be used as a precursor to producing activated carbons with a favorable surface area. To explore the potential advantage of the adsorbents used in this study, it is necessary to extend the present work to include the adsorption of the other emerging contaminants in water.

References

[1] V.K. Gupta, Suhas, Application of low-cost adsorbents for dye removal – a review, J. Environ. Manage., 90 (2009) 2313–2342.

[2] R. Kant, Adsorption of dye eosin from an aqueous solution on two different samples of activated carbon by static batch method, J. Water Resour. Prot., 4 (2012) 93–98.

[3] H. Zhang, F.Y. Zhang, Q. Huang, Highly effective removal of malachite green from aqueous solution by hydrochar derived from phycocyanin-extracted algal bloom residues through hydrothermal carbonization, RSC Adv., 7 (2017) 5790–5799.

[4] S. Gaspard, N. Passé-Coutrin, A. Durimel, T. Cesaire, V. Jeanne-Rose, Chapter 2 – Activated Carbon from Biomass for Water Treatment, S. Gaspard, M.C. Ncibi, Eds., Biomass for Sustainable Applications: Pollution Remediation and Energy, The Royal Society of Chemistry, London, 2014, pp. 46–105.

[5] H.N. Tran, H.-P. Chao, S.-J. You, Activated carbons from golden shower upon different chemical activation methods: synthesis and characterizations, J. Adsorpt. Sci. Technol., 36 (2016e) 95–113.

[6] K.J. Sun, J.C. Tang, Y.Y. Gong, H.R. Zhang, Characterization of potassium hydroxide (KOH) modified hydrochars from different feedstocks for enhanced removal of heavy metals from water, Environ. Sci. Pollut. Res., 22 (2015) 16640–16651.

[7] C. Falco, J.P. Marco-Lozar, D. Salinas-Torres, E. Morallón, D. Cazorla-Amorós, M.M. Titirici, D. Lozano-Castelló, Tailoring the porosity of chemically activated hydrothermal carbons: influence of the precursor and hydrothermal carbonization temperature, Carbon, 62 (2013) 346–355.

[8] P. Regmi, J.L.G. Moscoso, S. Kumar, X.Y. Cao, J.D. Mao, G. Schafran, Removal of copper and cadmium from aqueous solution using switchgrass biochar produced via hydrothermal carbonization process, J. Environ. Manage., 109 (2012) 61–69.

[9] X.D. Zhu, Y.C. Liu, C. Zhou, S.C. Zhang, J.M. Chen, Novel and high-performance magnetic carbon composite prepared from waste hydrochar for dye removal, ACS Sustainable Chem. Eng., 2 (2014) 969–977.

[10] A. Jain, R. Balasubramanian, M.P. Srinivasan, Tuning hydrochar properties for enhanced mesopore development in activated carbon by hydrothermal carbonization, Microporous Mesoporous Mater., 203 (2015) 178–185.

[11] Md. A. Islam, M.J. Ahmed, W.A. Khanday, M. Asif, B.H. Hameed, Mesoporous activated carbon prepared from NaOH activation of rattan (*Lacosperma secundiflorum*) hydrochar for methylene blue removal, Ecotoxicol. Environ. Saf., 138 (2017) 279–285.

[12] H.N. Tran, S.-J. You, H.-P. Chao, Y.-F. Wang, Sustainable Biochar Derived from Agricultural Wastes for Removal of methylene Green 5 from Aqueous Solution: Adsorption Kinetics, Isotherms, Thermodynamics, and Mechanism Analysis, CRC Press, 2017, p. 255.

[13] S. Nirmaladevi, N. Palanisamy, Preparation and adsorptive properties of activated carbon from *Acacia leucophloea* wood sawdust hydrochar by zinc chloride activation, Cellul. Chem. Technol., 53 (2019) 1029–1039.

[14] H.N. Tran, S.-J. You, H.-P. Chao, Fast and efficient adsorption of methylene green 5 on activated carbon prepared from new chemical activation method, J. Environ. Manage., 188 (2017) 322–336.

[15] J.-S. Cao, J.-X. Lin, F. Fang, M.-T. Zhang, Z.-R. Hu, A new absorbent by modifying walnut shell for the removal of anionic dye: kinetic and thermodynamic studies, Bioresour. Technol., 163 (2014) 199–205.

[16] Y. Liu, Z.F. Jing, T. Zhang, Q.Y. Chen, F.X. Qiu, Y.X. Peng, S. Tang, Fabrication of functional biomass carbon aerogels derived from sisal fibers for application in selenium extraction, Food Bioprod. Process., 111 (2018) 93–103.

[17] J.D. Dai, L. Qin, R.L. Zhang, A. Xie, Z.S. Chang, S.J. Tian, C.X. Li, Y.S. Yan, Sustainable bovine bone-derived hierarchically porous carbons with excellent adsorption of antibiotics: equilibrium, kinetic and thermodynamic investigation, Powder Technol., 331 (2018) 162–170.

[18] Y.K. Recepoğlu, N. Kabay, I. Yılmaz-Ipek, M. Arda, K. Yoshizuka, M. Nishihama, M. Yüksel, Equilibrium and kinetic studies on lithium adsorption from geothermal water by λ-MnO_2, Solvent Extr. Ion Exch., 35 (2018) 221–231.

[19] V. Ranjithkumar, S. Sangeetha, S. Vairam, Synthesis of magnetic activated carbon/α-Fe_2O_3 nanocomposite and its application in the removal of acid yellow 17 dye from water, J. Hazard. Mater., 164 (2014) 609–914.

[20] Y. Liu, Is the free energy change of adsorption correctly calculated?, J. Chem. Eng. Data, 54 (2009) 1981–1985.

[21] J.J. Salazar-Rabago, R. Leyva-Ramos, Novel biosorbent with high adsorption capacity prepared by chemical modification of white pine (*Pinus durangensis*) sawdust. Adsorption of Pb(II) from aqueous solutions, J. Environ. Manage., 169 (2016) 303–312.

[22] Z. Zhang, X.S. Luo, Y. Liu, P.X. Zhou, G.F. Ma, Z.Q. Lei, L. Lei, A low cost and highly efficient adsorbent (activated carbon) prepared from waste potato residue, J. Taiwan Inst. Chem. Eng., 49 (2015) 206–211.

[23] L.C.A. Oliveira, E. Pereira, I.R. Guimaraes, A. Vallone, M. Pereira, J.P. Mesquita, K. Sapag, Preparation of activated carbons from coffee husks utilizing $FeCl_3$ and $ZnCl_2$ as activating agents. J. Hazard. Mater., 165 (2009) 87–94.

[24] P. Gao, Z.-H. Liu, G. Xue, B. Han, M.-H. Zhou, Preparation and characterization of activated carbon produced from rice straw by $(NH_4)_2HPO_4$ activation, Bioresour. Technol., 102 (2011) 3645–3648.

[25] S. Karagöz, T. Tay, S. Ucar, M. Erdem, Activated carbons from waste biomass by sulfuric acid activation and their use on methylene blue adsorption, Bioresour. Technol., 99 (2008) 6214–6222.

[26] M. Auta, B.H. Hameed, Optimized waste tea activated carbon for adsorption of Methylene Blue and Acid Blue 29 dyes using response surface methodology, Chem. Eng. J., 175 (2011) 233–243.

[27] H. Sayğılı, F. Güzel, Y. Önal, Conversion of grape industrial processing waste to activated carbon sorbent and its performance in cationic and anionic dyes adsorption, J. Cleaner Prod., 93 (2015) 84–93.

[28] B.H. Hameed, A.L. Ahmad, K.N.A. Latiff, Adsorption of basic dye (methylene blue) onto activated carbon prepared from rattan sawdust, Dyes Pigm., 75 (2007) 143–149.

[29] H. Deng, L. Yang, G.H. Tao, J.L. Dai, Preparation and characterization of activated carbon from cotton stalk by microwave assisted chemical activation—application in methylene blue adsorption from aqueous solution, J. Hazard. Mater., 166 (2009) 1514–1524.
[30] P. Nowicki, J. Kazmierczak-Razna, R. Pietrzak, Physicochemical and adsorption properties of carbonaceous sorbents prepared by activation of tropical fruit skins with potassium carbonate, Mater. Des., 90 (2016) 579–585.
[31] Md. T. Uddin, Md. A. Rahman, Md. Rukanuzzaman, Md. A. Islam, A potential low cost adsorbent for the removal of cationic dyes from aqueous solutions, Appl. Water Sci., 7 (2017) 2831–2842.
[32] H.I. Chieng, N. Priyantha, L.B.L. Lim, Effective adsorption of toxic brilliant green from aqueous solution using peat of Brunei Darussalam: isotherms, thermodynamics, kinetics and regeneration studies, RSC Adv., 5 (2015) 34603–34615.
[33] M.T. Yagub, T.K. Sen, S. Afroze, H.M. Ang, Dye and its removal from aqueous solution by adsorption: a review, Adv. Colloid Interface Sci., 209 (2014) 172–184.
[34] K.A. Adegoke, O.S. Bello, Dye sequestration using agricultural wastes as adsorbents, Water Resour. Ind., 12 (2015) 8–24.
[35] F. Marrakchi, M. Bouaziz, B.H. Hameed, Adsorption of Acid Blue 29 and methylene blue on mesoporous K_2CO_3-activated olive pomace boiler ash, Colloids Surf., A, 535 (2017) 157–165.
[36] A. Purai, V.K. Rattan, Biosorption of leather dye (acid blue 193) from aqueous solution using ash prepared from cow dung, mango stone, parthenium leaves and activated carbon, Indian Chem. Eng., 54 (2012) 190–209.
[37] M.A.K. Megat Hanafiah, W.S.W. Ngah, S.H. Zolkafly, L.C. Teong, Z.A. Majid, Acid Blue 25 adsorption on base treated *Shorea dasyphylla* sawdust: kinetic, isotherm, thermodynamic and spectroscopic analysis, J. Environ. Sci., 24 (2012) 261–268.
[38] M.R.R. Kooh, M.K. Dahri, L.B.L. Lim, L.H. Lim, Batch adsorption studies on the removal of Acid Blue 25 from aqueous solution using *Azolla pinnata* and soya bean waste, Arabian J. Sci. Eng., 41 (2016) 2453–2464.
[39] A. Regti, M.R. Laamari, S.-E. Stiriba, M. El Haddad, The potential use of activated carbon prepared from Ziziphus species for removing dyes from waste waters, Appl. Water Sci., 7 (2017) 4099–4108.
[40] C.S. Gomes, J.S. Piccin, M. Gutterres, Optimizing adsorption parameters in tannery-dye-containing effluent treatment with leather shaving waste, Process Saf. Environ. Prot., 99 (2016) 98–106.
[41] S.E. Subramani, N. Thinakaran, Isotherm, kinetic and thermodynamic studies on the adsorption behavior of textile dyes onto chitosan, Proc. Saf. Environ. Prot., 106 (2017) 1–10.